Journal of Hazardous Materials 166 (2009) 821–829

Contents lists available at ScienceDirect

Journal of Hazardous Materials

journal homepage: www.elsevier.com/locate/jhazmat

Montmorillonite-supported magnetite nanoparticles for the removal of hexavalent chromium [Cr(VI)] from aqueous solutions

Peng Yuan[a], Mingde Fan[a,b], Dan Yang[a,b], Hongping He[a,*], Dong Liu[a,b], Aihua Yuan[c], JianXi Zhu[a], TianHu Chen[d]

[a] Guangzhou Institute of Geochemistry, Chinese Academy of Sciences, Guangzhou 510640, China
[b] Graduate School of Chinese Academy of Sciences, Beijing 100039, China
[c] School of Materials Science and Engineering, Jiangsu University of Science and Technology, Zhenjiang 212003, China
[d] School of Natural Resources & Environment, Hefei University of Technology, Hefei 230009, Anhui, China

ARTICLE INFO

Article history:
Received 10 October 2008
Received in revised form
25 November 2008
Accepted 25 November 2008
Available online 3 December 2008

Keywords:
Magnetite
Montmorillonite
Chromium
Adsorption
Transmission electron microscopy

ABSTRACT

Montmorillonite-supported magnetite nanoparticles were prepared by co-precipitation and hydrosol method. The obtained materials were characterized by X-ray diffraction, nitrogen adsorption, elemental analysis, differential scanning calorimetry, transmission electron microscopy and X-ray photoelectron spectroscopy. The average sizes of the magnetite nanoparticles without and with montmorillonite support are around 25 and 15 nm, respectively. The montmorillonite-supported magnetite nanoparticles exist on the surface or inside the interparticle pores of clays, with better dispersing and less coaggregation than the ones without montmorillonite support. Batch tests were carried out to investigate the removal mechanism of hexavalent chromium [Cr(VI)] by these synthesized magnetite nanoparticles. The Cr(VI) uptake was mainly governed by a physico-chemical process, which included an electrostatic attraction followed by a redox process in which Cr(VI) was reduced into trivalent chromium. The adsorption of Cr(VI) was highly pH-dependent and the kinetics of the adsorption followed the Pseudo-second-order model. The adsorption data of unsupported and clay-supported magnetite nanoparticles fit well with the Langmuir and Freundlich isotherm equations. The montmorillonite-supported magnetite nanoparticles showed a much better adsorption capacity per unit mass of magnetite (15.3 mg/g) than unsupported magnetite (10.6 mg/g), and were more thermally stable than their unsupported counterparts. These fundamental results demonstrate that the montmorillonite-supported magnetite nanoparticles are readily prepared, enabling promising applications for the removal of Cr(VI) from aqueous solution.

1. Introduction

During the last few decades, magnetite (Fe_3O_4) nanoparticles had attracted increasing research attentions in the field of environmental remediation [1]. For example, magnetite nanoparticles have shown favorable activities for the adsorption/reduction of quite a few heavy metal ions (e.g. Ni^{2+}, Cu^{2+}, Cd^{2+}, Zn^{2+}, and Cr^{6+}) [2–4]) and the catalytic degradation of some organic contaminants [5]. The application of magnetite nanoparticles in the environmental field is mainly due to their much better adsorption and reduction activities than their traditional macro- or micro-counterparts. In addition, magnetite can be easily separated and collected by an external magnetic field. This extraordinary advantage is specially useful for the recovery or reuse of the magnetite nanoparticles [6,7].

The coaggregation of nanoparticles often constitutes a challenge that nanomaterials have to be confronted, since the coaggregation decreases the effective surface area of nanoparticles and thus reduces their reaction activities. Several methods have been accordingly developed for overcoming the coaggregation and tailoring the size of the nanoparticles. Organized assemblies such as surfactants [8] and polymer matrix [9] were applied as dispersants to control the coaggregation and the size of the iron oxide nanoparticles. Supporting of magnetite nanoparticles on polymer [10,11], porous silica [12,13] and zeolites [14] during the preparation process were also found to be effective to prevent coaggregation. The resulting heterogeneous systems appeared better in recycling use with lower cost than their homogeneous counterparts. In this sense, it would be very interesting to synthesize supported magnetite nanoparticles and to explore the effect of the supporting materials on the related characteristics and activities of the nanoparticles.

Montmorillonite is a kind of natural 2:1 type layered clay mineral with high cation exchange capacity, swelling ability and high surface area. As a low-cost and readily available mineral with many

* Corresponding author. Tel.: +86 20 85290257; fax: +86 20 85290130.
E-mail address: hehp@gig.ac.cn (H. He).

0304-3894/$ – see front matter © 2008 Elsevier B.V. All rights reserved.
doi:10.1016/j.jhazmat.2008.11.083

excellent properties, montmorillonite has been widely used in a number of industrial branches. Due to its small particle size, bearing constant negative charge on surface and sheet-like structure, montmorillonite may be particularly suitable to be used as a support for the synthesis of magnetite nanoparticles. However, so far, few attempts to synthesize montmorillonite-supported magnetite composite could be found in literatures [15,16].

In the present study, montmorillonite-supported magnetite nanoparticles were prepared and the nanocomposites were further used for the removal of hexavalent chromium, to evaluate their feasibilities to be used as adsorbents in the environmental remediation. Cr(VI) is a highly toxic agent that is carcinogenic, mutagenic and teratogenic to living organisms [17]. Mainly existing in the forms of anions of chromate and dichromate in aqueous systems, Cr(VI) is usually released from various industrial operations, including metallurgy, leather tanning, chemical manufacturing, pulp production, ore and petroleum refining, metal corrosion, and electroplating [18]. Cr(VI)-containing wastewater from these processes is typically disposed by means of domestic sewage systems or even directly discharged to the aqueous bodies with little treatment in some undeveloped areas. A variety of methods have been developed for the removal of Cr(VI) from wastewater, such as adsorption, ion exchange, chemical precipitation, electro-deposition, photocatalysis reduction, solvent extraction, and reverse osmosis [3,19–21]. Among these methods chemical reduction followed by precipitation or adsorption is the most widely used technique [22]. With this method Cr(VI) is converted into trivalent chromium [Cr(III)] with much lower toxicity and limited hydroxide solubility. The reduction agents used for the converting process include iron sulfide and pyrite [23], ferrous iron [24], ferrite [25], various types of metallic iron and zero-valent iron [26–31], green rust [32], siderite [33] and magnetite [3,34,35]. However, less research attentions were paid to applying supported nano-sized magnetite as a reduction agent or an adsorbent for the treatment of Cr(VI).

Consequently, the objective of this study is to assess the feasibility of using montmorillonite-supported magnetite nanoparticles for removing Cr(VI) from aqueous solutions. For this purpose, two methods for synthesis of supported magnetite nanoparticles were adopted and the resulting materials were used in a series of batch experiments to investigate how the properties of materials and the experimental conditions (e.g. pH value and initial Cr(VI) concentrations) affect the related reaction mechanisms. All information obtained is based on a combined analysis of nitrogen adsorption–desorption isotherms, powder X-ray diffraction (PXRD), chemical analysis, differential scanning calorimetry (DSC), transmission electron microscope (TEM) and X-ray photoelectron spectroscopic (XPS) techniques.

2. Materials and methods

2.1. Materials

Raw Ca-montmorillonite from Hebei, China, was purified and classified by the conventional sedimentation method, and the <5 μm fraction was collected for further use. The purified Ca-montmorillonite has a chemical formula of $(Na_{0.05}Ca_{0.18}Mg_{0.10})[Al_{1.58}Fe_{0.03}Mg_{0.39}][(Si_{3.77}Al_{0.23})]O_{10}(OH)_2{\cdot}nH_2O$ and its cation exchange capacity (CEC) is 57.9 mmol/100 g. The Na-saturated montmorillonite (Mt), used for the preparation of supported magnetite nanoparticles, was prepared by ion exchange reaction between the purified Ca-montmorillonite and Na_2CO_3 following a commonly used procedure as previously described [36]. Analytical grade reagents such as ferric chloride hexa-hydrate ($FeCl_3{\cdot}6H_2O$, 99%), ferrous chloride tetra-hydrate ($FeCl_2{\cdot}4H_2O$, 99%) and ammonium hydroxide (NH_4OH) were used for the synthesis of magnetite. Potassium dichromate ($K_2Cr_2O_7$, 99%) was used for the preparation of Cr(VI) solution. A commercially micron-scaled magnetite (MicroMag) with average size of ca. 40 μm was used for comparison purpose.

The magnetite nanoparticles (Mag) were prepared by the following steps: the powder of $FeCl_3{\cdot}6H_2O$ and $FeCl_2{\cdot}4H_2O$, with a molar ratio of Fe(II)/Fe(III) = 1/2, were dissolved in distilled water that had just been deoxygenated by bubbling N_2 gas for 30 min. The amount of the totally added iron salt powder was about 3 g in 200 ml water. The solution was kept under N_2 protection and vigorously stirring for 5 min in a water bath at 60 °C. A solution of NH_4OH (1.5 M) was added dropwise into the Fe(II)/Fe(III) solution. Rightly after the addition of NH_4OH an initial brown precipitate was seen and afterwards a black precipitate was formed. The titration was stopped when the pH value of the mixture reached 8.0, and the mixture was aged for 30 min at 60 °C. The precipitate was isolated by using an external magnetic field and the supernatant was decanted. The obtained solid part was quickly washed four times with deionized and deoxygenated water and then dried at 40 °C under vacuum.

Two methods were applied to prepare the montmorillonite-supported magnetite nanoparticles. One was the co-precipitation route in which the montmorillonite powder was firstly added into a 1.5 M NaOH solution under stirring to make a suspension in which the content of montmorillonite is about 10%. Then the mixture was dropped into the ferric chloride/ferrous chloride solution, with a ratio of totally 3 mmol Fe per gram of montmorillonite. The followed preparation steps were conducted as those of the synthesis of Mag. The resultant sample was named as MagMt-P hereafter.

For the other preparation method the magnetite hydrosol was firstly synthesized and then loaded into the montmorillonite. The synthesis of the hydrosol of magnetite followed the previously proposed method [37]: magnetite nanoparticles were synthesized in distilled and deoxygenated water by a generally used method. After that, the precipitate of nanoparticles was washed four times, and then 0.01 M HCl solution was added into the precipitate under stirring to neutralize the anionic charges of the nanoparticles. The cationic colloidal nanoparticles were again separated by centrifugation (5 min, 4000 rpm) and peptized by adding water. The resultant was a clear and transparent cationic colloid (hydrosol) with pH value about 4.0 [37]. The hydrosol was left to stand for 3 h to settle out any residual solids and the dark-colored supernatant was separated for further preparation. In a run for the preparation of montmorillonite-supported magnetite nanoparticles, montmorillonite suspension was prepared with a concentration of 1 g of montmorillonite per 20 ml of water, and then the magnetite hydrosol with equivalent volume was added to the montmorillonite suspension followed by stirring for 30 min. The mixture was centrifuged at 4000 rpm for 5 min, and it was observed that the supernatant liquid became colorless. This indicated that the magnetite nanoparticles were completely adsorbed by the montmorillonite particles. The colorless supernatant was discarded and further magnetite hydrosol was added. The above stirring and centrifugation steps were repeated several times until the supernatant liquid did not become colorless anymore, indicating a saturated adsorption of magnetite hydrosol onto the montmorillonite was achieved. The resultant solid was separated and dried at 40 °C under vacuum. The obtained montmorillonite-supported magnetite was referred to as MagMt-H.

All of the prepared samples were kept on a vacuum desiccator before being used for adsorption experiments. To test the stability of the supported/unsupported magnetite nanoparticles over a long term, a portion of each synthesized sample was placed into a covered container with ambient condition and then taken over a period of 2 years. The obtained samples were differentiated by the suffix -T, for example, Mag-T.

2.2. Adsorption experiments

In a typical run, 0.5 g adsorbent was added into 100 ml of Cr(VI) solution in a 125 ml high density poly(ethylene) (HDPE) bottle. No buffer was added in these experiments. The Cr(VI) solution was prepared by dissolving $K_2Cr_2O_7$ in distilled water. The pH value was adjusted by 0.1 M HNO_3 and 0.1 M NaOH solution. For the kinetics tests, the mixture in the HDPE bottle was strongly shaken at a rate of 160 rpm in an oscillator to ensure a complete mixing. The contact time was in the range from 2 to 120 min. At timed intervals, samples were taken by HDPE 3 ml syringe and filtered through a 0.2 μm cellulose acetate syringe filters. The Cr(VI) content in the filtered solution was measured by using a Shimadzu UV-260 Spectrophotometer according to the determination procedure described in the literature [38]. The experiments for obtaining adsorption isotherms followed a very similar procedure except for the equilibrium time was fixed as 120 min. All adsorption experiments were conducted at room temperature (25 ± 2 °C) unless noted, and all of the adsorption results were corrected by blank tests in which no adsorbent was added into the Cr(VI) solution. The amount of Cr(VI) adsorbed per unit mass of the adsorbent, q (mg/g), was calculated by using the expression: $q = (C_0 - C_t)/m$, where C_0 and C_t (mg/L) are the concentration of Cr(VI) in the reaction solution before and after treatment, respectively, and m (g) is the amount of adsorbents in 1 l of Cr(VI) solution. The removal efficiency of Cr(VI), E (%), was calculated using the equation: $E = [(C_0 - C_t)/C_0] \times 100$.

2.3. Characterization

A Rigaku D/Max 2200 VPC diffractometer, equipped with a graphite-monochromatized Cu Kα radiation course (λ = 0.154 nm) under target voltage 40 kV and current 30 mA was used to obtain the XRD patterns. All samples were recorded between 5 and 80° (2θ) at a scanning rate of 4°/min. The chemical compositions of the samples were determined using a PE-3100 atomic absorption spectrometer (AAS). N_2 adsorption–desorption isotherms were measured on a Micromeritics ASAP 2020 system at liquid nitrogen temperature. The samples were outgassed at both 110 and 350 °C for 8 h before measurement but no large difference between the obtained results were observed. So only the data corresponding to 350 °C outgassing are presented herein. The specific surface area, S_{BET}, of the sample was calculated by using the multiple-point Brunauer–Emmett–Teller (BET) method [39] and the total pore volume, V_{pore}, was evaluated from nitrogen uptake at a relative pressure of ca. 0.97. The t-plot method was used to calculate the microporous and external surface areas. The pore size distribution was computed by using the Barrett–Joyner–Halenda (BJH) method [40].

TEM images were obtained on a Philips CM120 electron microscope operating at an acceleration voltage of 120 kV. The specimens for TEM observation were prepared by the following procedure. The sample was ultrasonically dispersed in ethanol for 5 min, and then a drop of sample suspension was dropped onto a carbon-coated copper grid, which was left to stand for 10 min and transferred into the microscope.

DSC characterization was performed on a Netzsch STA 409 PC instrument. Approximately 10 mg of finely ground sample was heated in a corundum crucible with a heating rate of 5 °C/min under air atmosphere. XPS analysis was performed on a Kratos AXIS Ultra with a monochromatic Al X-ray source at 150 W. Each analysis started with a survey scan from 0 to 1200 eV with a dwell time of 100 ms, pass energy of 160 eV at steps of 1 eV with one sweep. For the high-resolution analysis, the number of sweeps was increased, the pass energy was lowered to 20 eV at steps of 100 meV and the dwell time was changed to 250 ms.

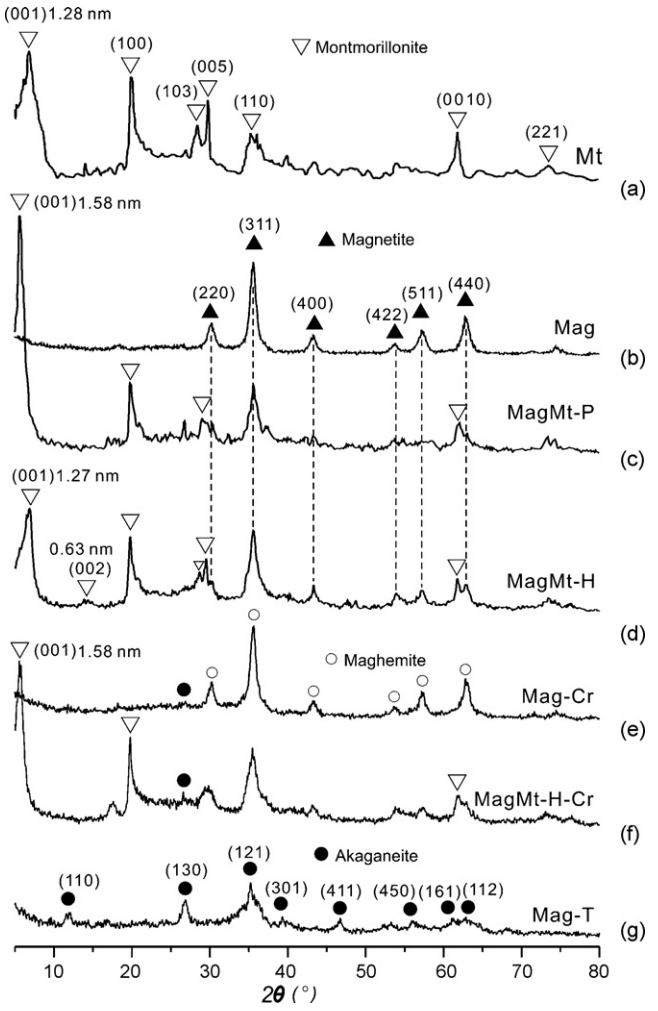

Fig. 1. XRD patterns of the montmorillonite and the unsupported/supported magnetite samples.

3. Results and discussion

3.1. Characterization of the supported/unsupported magnetite nanoparticles

Displayed as Fig. 1a is the XRD pattern of Mt, which represents a typical pattern of Na^+-exchanged montmorillonite indicated by the d(0 0 1) value of 1.28 nm. The diffraction pattern of synthesized magnetite nanoparticles (Fig. 1b) exhibits distinct plane distances of 0.296, 0.253, 0.209, 0.161, and 0.148 nm, which are well consistent with the referenced data of 0.297, 0.253, 0.209, 0.162, and 0.149 nm for (2 2 0), (3 1 1), (4 0 0), (5 1 1) and (4 4 0) plane distances, respectively [41]. Fig. 1c and d present the XRD patterns of montmorillonite-supported magnetite prepared via co-precipitation (MagMt-P) and hydrosol method (MagMt-H). MagMt-P shows a d(0 0 1) spacing of 1.58 nm (Fig. 1c), implying the interlayered Na^+ has been replaced by some primary hydrolyzed cations of iron during the preparation process [42]. In contrast, the d(0 0 1) spacing (1.28 nm) remains unchanged in the pattern of MagMt-H (Fig. 1d). This reflects that magnetite particles did not enter into the clay interlayer spaces via ion exchange, possibly resulted from the much bigger size of the magnetite hydrosol than that could be accommodated by the clay interlayer spaces. Moreover, the content of magnetite nanoparticles in MagMt-H is significantly higher than that of MagMt-P, based on a semi-quantitatively calculation by use of deconvolution of XRD peaks.

Table 1
The total Fe_2O_3 content and the porous structural data of the prepared samples.

Sample	Mag	Mt	MagMt-P	MagMt-H
Fe_2O_3 (%)	96.0	0.5	22.5	51.4
S_{BET} (m^2/g)	86.6	84.0	73.1	84.5
[a]$S_{ext.}$ (S_{micro}) (m^2/g)	82.7 (3.9)	71.8 (12.2)	70.7 (2.4)	84.5 (0.0)
V_{pore} (cm^3/g)	0.32	0.20	0.16	0.24

[a] $S_{ext.}$ = external surface area, evaluated from *t*-plot; surface area of micropore (S_{micro}) is obtained by subtracting $S_{ext.}$ from total surface area (S_{BET}).

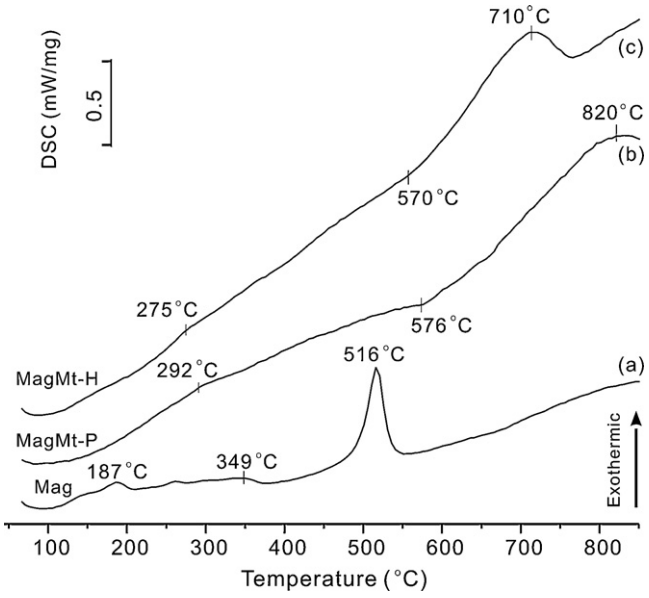

Fig. 2. DSC curves of the montmorillonite-supported/unsupported magnetite samples.

This is in accordance with the chemical analysis result (Table 1) that the content of Fe_2O_3 in MagMt-P (22.5%, wt.%) is lower than that in MagMt-H (51.4%).

As shown in the DSC curve of Mag (Fig. 2a), an exothermic signal at ca. 187 °C is resolved, which corresponds to the beginning temperature of the transformation from magnetite to maghemite (γ-Fe_2O_3) [43]. This transformation appears a multi-step process, which is composed of gradual transformation of the magnetite nanoparticles with different sizes and ends at ca. 349 °C (Fig. 2a). The exothermic signal at 516 °C is attributed to the transformation from maghemite to hematite (α-Fe_2O_3). These two thermal events are consistent with the previously reported phase-transformation temperature range of magnetite [41,43,44]. As compared to Mag, MagMt-P exhibits much weaker signals of the transformation from magnetite to maghemite, which begins at about 292 °C (Fig. 2b), and finishes before 500 °C despite that the accurate endpoints is difficult to be anchored. Meanwhile, exothermic signal of the phase-transformation from maghemite to hematite for MagMt-P centers at about 820 °C. The increase of the phase-transformation temperature of MagMt-P relative to those of Mag suggests the supporting of montmorillonite places a positive influence on increasing the thermal stabilities of the magnetite nanoparticles. This is probably due to the nanoparticles were effectively separated by the clay flakes, and therefore many of them were prevented from aggregating and further transforming. A similar phenomenon was also found in the heterogeneous systems of iron oxide and titanium oxide delaminated-pillared clay and the related mechanisms had been discussed in detail [45,46].

The DSC curve of MagMt-H is generally analogous to that of MagMt-P (Fig. 2c), but the temperature of phase-transformation from maghemite to hematite was advanced to 710 °C. This is due to the montmorillonite particles accounting for a much smaller proportion in MagMt-H than in MagMt-P, resulting in a less thermal stability-increasing effect. On the other hand, MagMt-P shows an endothermic signal around 576 °C that is assigned to the dehydroxylation process of the montmorillonite support [47]. This signal is stronger than its counterpart (around 570 °C, Fig. 2c) in the DSC curve of MagMt-H, providing a further evidence for the higher content of montmorillonite in MagMt-P than in MagMt-H.

As revealed by the TEM image (Fig. 3a), the synthesized magnetite nanoparticles in Mag dramatically coaggregated together. The nanoparticles have an average size around 25 nm. The supported magnetite nanoparticles showed decreased sizes (Fig. 3b and c) of ca. 20 and 15 nm for MagMt-P and MagMt-H, respectively. And the magnetite nanoparticles in MagMt-H were better dispersed at the surface of clay than those in MagMt-P. These comparisons suggest that the montmorillonite-supported magnetite prepared via hydrosol route is more advantageous than that via co-precipitate route in enhancing the dispersion and decreasing the size of magnetite nanoparticles. This result may be due to that in the hydrosol preparation route the positively charged magnetite hydrosol specifically attracted the negatively charged clay surface by electrostatic interactions, whereas in the co-precipitate route many magnetite nanoparticles were just unintentionally mixed with the shells so that the linkage between them was not sufficiently tight.

The nitrogen adsorption–desorption isotherms of the samples are shown in Fig. 4. The isotherms of Mag and Mt belong to the type II with H3 hysteresis loops, according to IUPAC-classification [39]. The hysteresis loop of this isotherm is associated with the filling and emptying of the mesopores by capillary condensation. For Mag, the mesopores should be interparticle pores among magnetite nanoparticles since magnetite is actually nonporous as already known. For Mt, the mesoporous structure should be resulted from the stacking of platy montmorillonite particles in three-dimension space. Represented in the inset of Fig. 4 is the pore size distribution

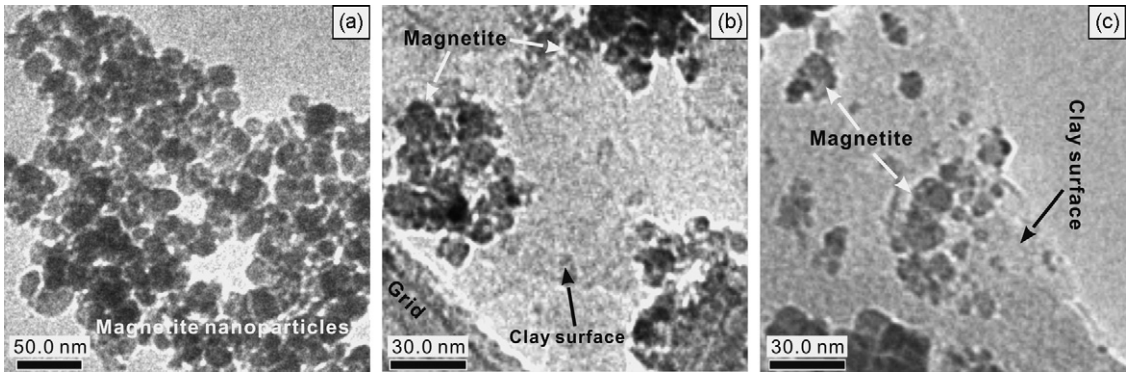

Fig. 3. TEM images of (a) Mag; (b) MagMt-P; and (c) MagMt-H.

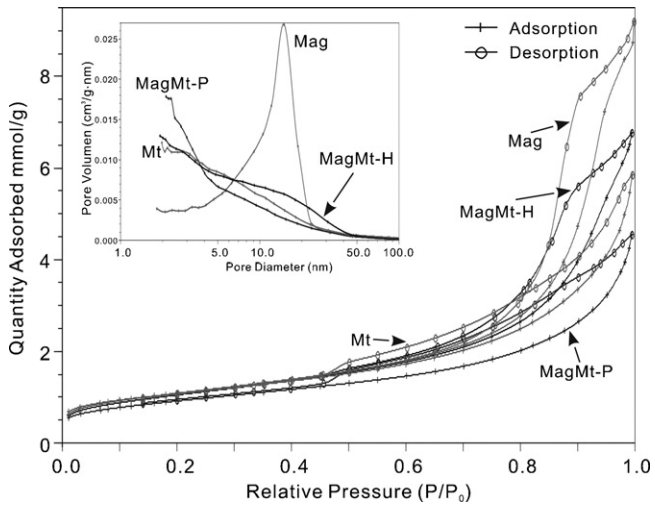

Fig. 4. Nitrogen adsorption–desorption isotherms and PSD curves (the insert) of montmorillonite and the unsupported/montmorillonite-supported magnetite samples.

(PSD) curves calculated from the BJH method. The primary peak at ca. 15 nm in the curve of Mag corresponds to the main pore population in Mag, and can be readily identified as the interspaces among magnetite particles. In contrast, sample Mt shows a broader pore distribution in which pores with different sizes coexist.

MagMt-P exhibits similar-shaped isotherms and PSD curves to those of Mt whereas its porosity (Table 2) was reduced when compared to Mt. This implies that the loaded magnetite nanoparticles are not well dispersed on the clay surface, resulting in a decrease of the entire effective surface area. The isotherm shape of MagMt-H is more close to that of Mag with less developed hysteresis loop, but the related PSD curve shows that the originally primary peak at ca. 15 nm almost diminished. This result indicates the mesopores resulting from interspaces of magnetite nanoparticles were dramatically reduced, reflecting the coaggregation of the nanoparticles was lowered obviously in MagMt-H. This presumption is evidenced by the fact that the porosity of MagMt-H (Table 2) did not show significant decrease, compared to that of Mag, despite that the loading content of magnetite in MagMt-H is much higher than in MagMt-P. These above observations are in good agreement with the XRD, the chemical analysis, and the TEM results.

3.2. Effect of pH values on the removal of Cr(VI)

Due to its superiority over MagMt-P in the dispersion performance of magnetite nanoparticles, MagMt-H was selected for the adsorption tests. To investigate the effects of pH on the adsorption, the initial pH values were adjusted to the range of 2.0–9.0 before the adding of the adsorbent into the solution. The initial Cr(VI) concentration was set as 50 mg/l and the agitation time was 120 min. The maximum removal efficiency (ca. 99.8%) of Mag was found at pH 2.0–2.5. A dramatic decrease occurred at pH 3–4, followed by a gradual decrease in the pH range of 4–9 (Fig. 5a). This result is well consistent with the previous report [3], and can be explained as follows: different species of Cr(VI) (e.g. $Cr_2O_7^{2-}$, $HCrO_4^-$, $Cr_3O_{10}^{2-}$, $Cr_4O_{13}^{2-}$) coexist at acidic pH condition. The predominant Cr(VI) species at pH 2–3 is $HCrO_4^-$, which is favorable adsorbed since it has a low adsorption free energy [48]. The significant decrease of the Cr(VI) uptake with the increase of pH values is due to the increscent concentration of OH^- ions presenting in the reaction mixture, which compete with Cr(VI) anions for the adsorption sites and thus reduce the removal efficiency of Mag. Moreover, the surfaces of magnetite nanoparticles in aqueous solution are positively charged and anion adsorption favored at a pH value below the pH_{ZPC} (the zero point of charge, ~8.3) [3] of magnetite, and vice versa, negatively charged and cation adsorption favored when pH is above the pH_{ZPC}.

Table 2
Kinetics constants for the adsorption of Cr(VI) on the various adsorbents.

Samples	R^2	K_p [g/(mg min)]	q_e (mg/g)	$t_{1/2}$ (min)
Mag	1	0.60	9.86	0.17
MagMt-H	0.999	0.07	7.56	1.92
MicroMag	0.997	0.08	4.95	2.38

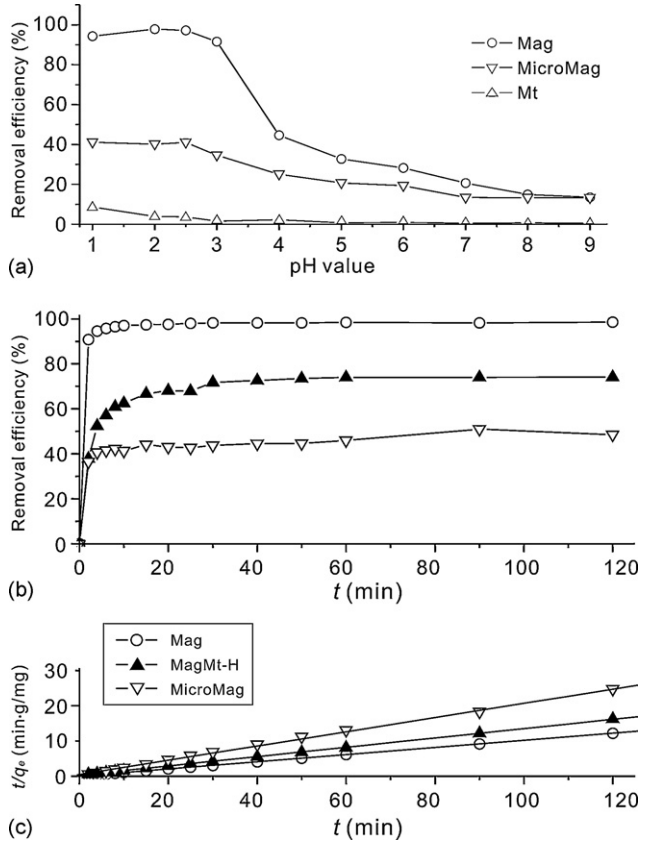

Fig. 5. (a) Effect of initial solution pH values on the removal of Cr(VI) on Mag, MicroMag, and Mt; (b) effect of agitation time on the removal of Cr(VI) using Mag, MicroMag, and MagMt-H; and (c) Pseudo-second-order linear plot for the adsorption of Cr(VI) on the various adsorbents.

As a result, an increase of pH value will make the Mag surfaces less positively charged, greatly weakening the electrostatic attraction between magnetite particles and negatively charged Cr(VI) anions. The uptake of Cr(VI) on micro-scaled MicroMag show a similar pH-dependency to that of Mag, but with much lower removal efficiency (the maximum is about 40% of Mag's) at the same pH values (Fig. 5a). This is due to that the amount of the adsorption sites in MicroMag is substantially less than those in Mag.

The maximum removal efficiency (ca. 10%) by Mt occurs at pH 1.0 (Fig. 5a). Such low adsorption of Cr(VI) on Mt should mainly be ascribed to that the "face" surface of montmorillonite bears constant negative charge resulting from the isomorphous substitutions in Si–O tetrahedrons or Al–O octahedrons [47]. Accordingly, The negatively charged montmorillonite layers are not favored to the adsorption of the anionic Cr(VI) species. With the increase of pH values, the removal efficiency of Mt further decreased (Fig. 5a). This can be explained by the process of electrostatic repulsion discussed above, since the "edge" of montmorillonite sheets is pH-dependent

and have more negative charges when the pH values is increased. Considering the removal efficiency of Mt remained at a low level throughout the whole pH range, all subsequent adsorption experiments herein were conducted at pH of 2.5, the optimum pH for adsorption of Cr(VI) on Mag.

3.3. Kinetics of adsorption and effect of initial Cr(VI) concentration

The adsorption of Cr(VI) by Mag and MagMt-H as a function of time at initial Cr(VI) concentration of 50 mg/l is displayed in Fig. 5b. The rate of Cr(VI) uptake was quite high toward the beginning, followed by a much slower subsequent removal rate and at last leading to an equilibrium condition. About 90% of the Cr(VI) was removed by Mag during the first 2 min of the reaction, while only a small part of the additional removal occurred during the rest contact time (Fig. 5b). MagMt-H shows a similar rapid adsorption for Cr(VI), in which the uptake of more than 90% of the totally adsorbed Cr(VI) species was finished in the first 5 min (Fig. 5b). The rapid adsorption of Cr(VI) by Mag and MagMt-H may be attributed to the external surface adsorption. This suggests that most of the adsorption sites of the nanoparticles exist in the exterior of the adsorbent and are easily accessible by the Cr(VI) species, thus resulting in a rapid approach to equilibrium. For both adsorbents, the adsorption equilibrium was achieved in 1 h. In comparison, this equilibrium time is close to that of maghemite nanoparticle (about 20–60 min) [49], and is much higher than those of MicroMag (~90 min, Fig. 5b), peat (~6 h) [50], volcanic ash soil (~6 h) [51], and activated carbon (about 10–70 h) [52,53].

The kinetics of the adsorption process shown in Fig. 5 was simulated using the Pseudo-second-order model [54,55] with the rate expression given by

$$\frac{dq_t}{Mt} = k_p(q_e - q_t)^2 \quad (1)$$

where k_p is the second order rate constant (g/mg min), q_t and q_e are the amount of Cr(VI) adsorbed per unit mass (mg/g) at any time (t) and at equilibrium, respectively. By integrating Eq. (1) and using the boundary conditions of $t = 0$ to t and $q_t = 0$ to q_t, the linear form of the equation could be obtained as

$$\frac{t}{q_t} = \frac{1}{(k_p q_e^2)} + \frac{t}{q_e} \quad (2)$$

The plot of t/q_t versus t gives a linear plot, which allows computation of q_e and k_p. As presented in Fig. 5c, the sorption of Cr(VI) onto both Mag and MagMt-H fits the Pseudo-second order model quite well, since the correlation coefficients (R) for the linear plots of t/q_t against time from the Pseudo-second order rate law are greater than 0.99 for both systems (Table 2). This result indicates that this sorption system is a Pseudo-second-order reaction, implying the rate-limiting step may be a chemical sorption involving valency forces through sharing or exchanging of electrons between sorbent and sorbate [54].

3.4. Effect of initial concentration of Cr(VI) and the adsorption isotherms

To explore the effects of initial concentrations on the removal efficiency of Cr(VI), various Cr(VI) concentrations were applied with a constant adsorbent amount (5 g/l) and contact time (120 min). The percentages of Cr(VI) removal decrease with the increase of the initial concentration of Cr(VI) for both Mag and MagMt-H (Fig. 6a). This is because the totally available adsorption sites of adsorbents with fixed dosage may be insufficient within selected time when the solution with high Cr(VI) concentration was used [33].

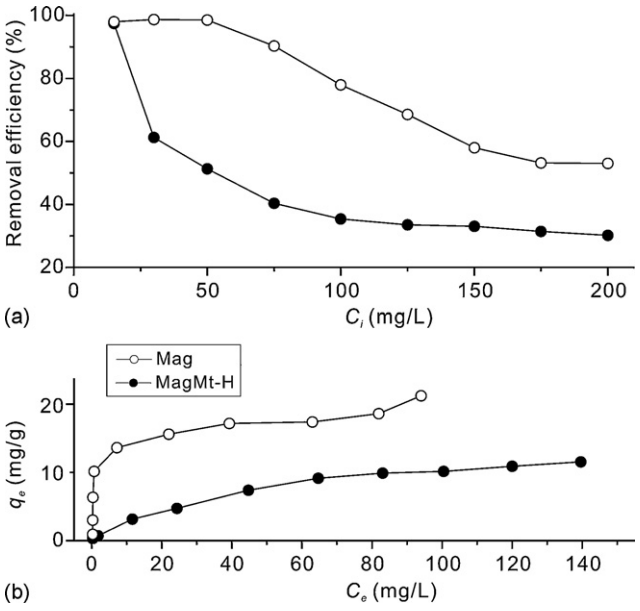

Fig. 6. (a) Effect of different initial Cr(VI) concentrations on the removal of Cr(VI) by Mag and MagMt-H; and (b) the Cr(VI) adsorption isotherms of Mag and MagMt-H.

Fig. 6b shows the adsorption isotherms of the adsorption of Cr(VI) onto Mag and MagMt-H. Both the Langmuir and the Freundlich equation were used to quantitatively describe the Cr(VI) uptake. The linear form of the Langmuir plot is given as

$$\frac{C_e}{Q_e} = \frac{1}{(bQ_m)} + \left(\frac{1}{Q_m}\right) C_e \quad (3)$$

where b and Q_m (mg/g) are the Langmuir constant and the monolayer adsorption capacity, respectively, and C_e (mg/L) is the equilibrium concentration of the Cr(VI) in liquid phase. The Freundlich model is an empirical equation with its linear form expressed as

$$\log Q_e = \log K_f + \left(\frac{1}{n}\right) \log C_e \quad (4)$$

where Q_e (mg/g) is the amount of Cr(VI) uptake at equilibrium; K_f and n are the Freundlich constants related to adsorption capacity and the adsorption intensity, respectively. The adsorption coefficients computed from above two models are shown in Table 3.

It is seen that the adsorption isotherms of both Mag and MagMt-H can be fit by the Langmuir and the Freundlich models. However, the Langmuir model shows to be better than the Freundlich model for fitting the adsorption isotherm of Mag, whereas MagMt-H well fit with both models. For both samples, the adsorption intensity given by the Freundlich coefficient, $1/n$, is <1. This reflects that the adsorption of Cr(VI) on the adsorbents is favorable. The Langmuir equilibrium coefficients, b and Q_m, of Mag are much higher than those of MagMt-H (Table 3), implying a stronger binding of Cr(VI) on Mag than on MagMt-H.

3.5. Adsorption mechanisms

Fig. 7 exhibits the XPS spectra of chromium and iron from the adsorbent surface after adsorption at pH 2.5. The Cr-loaded adsorbents were highlighted in the sample names by adding a suffix "-Cr", i.e., Mag-Cr and MagMt-H-Cr. The Cr2p XPS spectra of Mag-Cr and MagMt-H-Cr display two peaks centered at 577.8 and 586.8 eV (Fig. 7a), assigned to $Cr2p_{3/2}$ and $Cr2p_{1/2}$, respectively [41]. These peaks are typically assigned to Cr(III), indicating that the Cr(VI) in solution had been adsorbed onto the surface of the adsorbents and then reduced to Cr(III) by a heterogeneous redox process

Table 3
Freundlich and Langmuir adsorption parameters for adsorption of Cr(VI) on Mag and MagMt-H.

Adsorbents	Langmuir equation parameters			Freundlich equation parameters		
	b	Q_m (mg/g)	R^2	K_f	$1/n$	R^2
Mag	0.262	20.16	0.998	4.90	0.34	0.729
MagMt-H	0.030	13.88	0.965	1.62	0.38	0.984

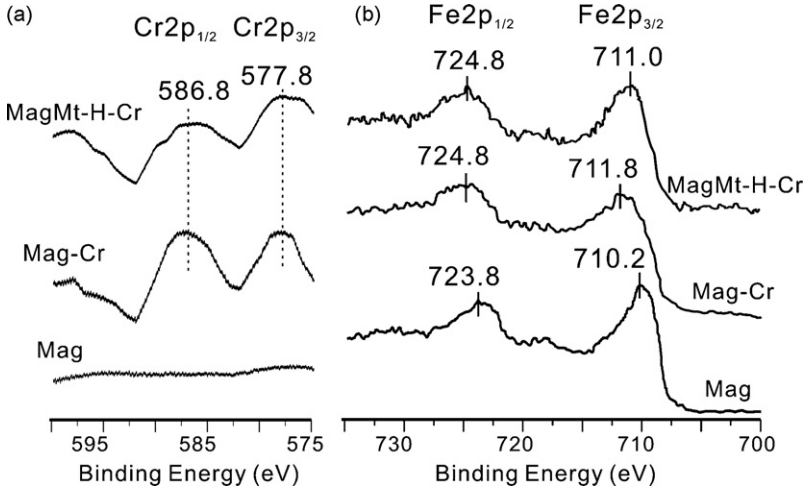

Fig. 7. (a) Fe2p and (b) Cr2p XPS spectra of the synthesized magnetite and Cr-loaded samples.

[56,57]. Meanwhile, the Fe2p XPS spectra of Mag-Cr and MagMt-H-Cr showed only fully oxidized iron on the surface, characteristic of the $2p_{3/2}$ peaks centered at ca. 711.8 and 711.0 eV (Fig. 7b), respectively [58]. However, in the Fe2p XPS spectrum of Mag (Fig. 7b), the $2p_{3/2}$ peak is centered at ca. 710.2 eV and the $2p_{1/2}$ peak is at ca. 723.8 eV, which matches well with the data of referenced magnetite [41,58]. Furthermore, the values of the binding energy of Fe($2p_{3/2}$) and Fe($2p_{1/2}$) in Mag-Cr and MagMt-H-Cr were higher than that in Mag. The increase of the binding energy of Fe($2p_{1/2}$) was previously suggested as an indication of the substitution of Cr(III) for Fe^{3+} in Cr-substituted magnetites [58,59], so possibly the isomorphic substitution of Fe^{3+} by Cr^{3+} took place in Mag-Cr and MagMt-H-Cr, considering that Fe^{3+} and Cr^{3+} have similar ionic radii (0.067 nm for Fe^{3+} and 0.065 nm for Cr^{3+}) and the substitution of Cr^{3+} for Fe^{3+} is thermodynamically favored [58]. However, further experimental evidences are still needed for confirming the occurrence of the isomorphic substitution.

As shown in Fig. 1e, the XRD pattern of Mag-Cr (Fig. 1e) should be assigned to the pattern of maghemite-like phase rather than magnetite, although both of the two phases have spinel-type structure and exhibit very similar XRD patterns. This assignment is evidenced by the XPS result that Mag-Cr shows a fully oxidized state, and the relevant DSC curve of Mag-Cr (not shown) also supports the attribution since the signals of phase-transformation from magnetite to maghemite were not observed any more. Likewise the iron oxide phase in MagMt-H-Cr should be maghemite. In addition, a small amount of akaganeite (β-FeOOH) was found to exist in both Mag-Cr and MagMt-H-Cr as indicated by the XRD patterns (Fig. 1e and f). It should be resulted from the reaction between magnetite and the chlorine-contained solution [41,60]. Furthermore, there are no new Cr-contained phases (e.g. chromite, $FeCr_2O_4$) as previously reported [3], found in either Mag-Cr or MagMt-H-Cr. These above results indicate that the magnetite was oxidized into maghemite during the adsorption of Cr(VI), and the resulting Cr(III) species may exist in the surface of the final maghemite-like solid.

To compare the Cr(VI) removal efficiency of unsupported/supported magnetite, the amount of Cr(VI) adsorbed per unit mass (g) of actual magnetite content, $q_{e\text{-}s}$, was calculated by the obtained Fe_2O_3 content (Table 1) and the values of q_e (Table 2) derived from the adsorption kinetic simulation. The values of $q_{e\text{-}s}$ for Mag and MagMt-H were obtained as 10.6 and 15.3 mg/g, respectively. This result reflects that the magnetite nanoparticles supported on montmorillonite have much higher efficiency on the adsorption and reduction for Cr(VI) than the unsupported ones. This is in accordance with the fact that magnetite nanoparticles were better dispersed than their homogeneously unsupported counterparts. Further advantages of the heterogeneous montmorillonite-supported magnetite can be postulated, for instance, this material may be much more readily to be pelletized than the unsupported magnetite nanoparticles, and thus be advantageous in actual industrial processes such as recycling and reuse. Moreover, the common uses of montmorillonite as catalytic supports and filler are of help for extending the related applications of supported magnetite.

It is also noteworthy that the supporting treatment places an influence on enhancing the stability of the magnetite nanoparticles for storage. As indicated by Fig. 1g, sample Mag-T, obtained by placing sample Mag under ambient condition for 2 years, showed a XRD pattern corresponding to akaganeite. The formation of akaganeite results from the long-term reaction between the magnetite and the water in ambient condition, as reported in literature [60]. However, the XRD pattern of MagMt-H-T (not shown) just resembles that of MagMt-H, indicating the magnetite nanoparticles were prevented from transforming into akaganeite. A possible explanation to this observation is that the clay particles adsorbed the ambient water and effectively reduced the contact between water molecules and the magnetite. This property of montmorillonite-supported magnetite is useful for its storage and transportation.

4. Conclusions

Montmorillonite-supported magnetite nanoparticles can be prepared by both co-precipitation and hydrosol method. The supported magnetite nanoparticles synthesized via hydrosol method

are shown to be better dispersive than those synthesized via co-precipitation method and the unsupported magnetite nanoparticles.

The Cr(VI) uptake onto these synthesized magnetite nanoparticles was a physico-chemical process, including an electrostatic attraction followed by a redox process in which Cr(VI) was reduced into trivalent chromium. For a given sample, the adsorption of Cr(VI) was strongly affected by the pH values and the kinetics of the adsorption followed the Pseudo-second-order model. The adsorption data of unsupported/supported magnetite nanoparticles fit well with the Langmuir and Freundlich isotherm equations. The montmorillonite-supported magnetite nanoparticles synthesized via hydrosol method exhibited a better adsorption capacity per unit mass of magnetite, and a better stability for storage, than their unsupported counterparts. During the adsorption of Cr(VI) onto magnetite nanoparticles, Cr(VI) not only can be reduced Cr(III) with less toxicity than Cr(VI) but also can be fixed into the iron oxide. This is of high importance for the application of magnetite in the field of environmental remediation.

These preliminary results indicate that both the montmorillonite-supported magnetite nanoparticles are readily prepared, enabling promising applications for the removal of Cr(VI) from aqueous solution. Taking montmorillonite as a support is useful on tailoring the dispersing and the aggregation behavior of magnetite nanoparticles, and thus is of help for their pelletization, storage, and some related applications.

Acknowledgements

This is a contribution (No. IS-1013) from GIGCAS. Financial supports from National Science Fund for Distinguished Young Scholars (Grant No. 40725006), the Knowledge Innovation Program of the Chinese Academy of Sciences (Grant No. Kzcx2-yw-112) and National Natural Science Foundation of China (Grant No. 40672036) are gratefully acknowledged.

References

[1] A.F. Ngomsik, A. Bee, M. Draye, G. Cote, V. Cabuil, Magnetic nano- and microparticles for metal removal and environmental applications: a review, Comptes Rendus Chimie 8 (2005) 963–970.
[2] L.C.A. Oliveira, R.V.R.A. Rios, J.D. Fabris, K. Sapag, V.K. Garg, R.M. Lago, Clay-iron oxide magnetic composites for the adsorption of contaminants in water, Appl. Clay Sci. 22 (2003) 169–177.
[3] J. Hu, I.M.C. Lo, G. Chen, Removal of Cr(VI) by magnetite nanoparticle, Water Sci. Technol. 50 (2004) 139–146.
[4] S.S. Banerjee, D.H. Chen, Fast removal of copper ions by gum Arabic modified magnetic nano-adsorbent, J. Hazard. Mater. 147 (2007) 792–799.
[5] C.L. Chun, R.M. Hozalski, T.A. Arnold, Degradation of drinking water disinfection byproducts by synthetic goethite and magnetite, Environ. Sci. Technol. 39 (2005) 8525–8532.
[6] N.A. Booker, D. Keir, A.J. Priestley, C.B. Ritchie, D.L. Sudarmana, M.A. Woods, Sewage clarification with magnetite particles, Water Sci. Technol. 23 (1991) 1703–1712.
[7] J.D. Orbell, L. Godhino, S.W. Bigger, T.M. Nguyen, L.N. Ngeh, Oil spill remediation using magnetic particles—an experiment in environmental technology, J. Chem. Educ. 74 (1997) 1446–1448.
[8] N. Feltin, M.P. Pileni, New technique to make ferrite nanosized particles, J. Phys. IV 7 (1997) 609–610.
[9] R.F. Ziolo, E.P. Giannelis, B.A. Weinstein, M.P. Ohoro, B.N. Ganguly, V. Mehrotra, M.W. Russell, D.R. Huffman, Matrix-mediated synthesis of nanocrystalline gamma-Fe_2O_3—a new optically transparent magnetic material, Science 257 (1992) 219–223.
[10] A.A. Novakova, V.Y. Lanchinskaya, A.V. Volkov, T.S. Gendler, T.Y. Kiseleva, M.A. Moskvina, S.B. Zezin, Magnetic properties of polymer nanocomposites containing iron oxide nanoparticles, J. Magn. Magn. Mater. 258 (2003) 354–357.
[11] Y.S. Kang, S. Risbud, J. Rabolt, P. Stroeve, Brewster angle microscopy study of a magnetic nanoparticle/polymer complex at the air/water interface, Langmuir 12 (1996) 4345–4349.
[12] M.J. Zhang, Q. Zhang, T. Itoh, M. Abe, Ferrite plating on porous silica microspheres for ultrasonic contrast agents, IEEE Trans. Magn. 30 (1994) 4692–4694.
[13] I.J. Bruce, J. Taylor, M. Todd, M.J. Davies, E. Borioni, C. Sangregorio, T. Sen, Synthesis, characterisation and application of silica-magnetite nanocomposites, J. Magn. Magn. Mater. 284 (2004) 145–160.
[14] M. Arruebo, R. Fernandez-Pacheco, S. Irusta, J. Arbiol, M.R. Ibarra, J. Santamaria, Sustained release of doxorubicin from zeolite-magnetite nanocomposites prepared by mechanical activation, Nanotechnology 17 (2006) 4057–4064.
[15] N.B. Shrigadi, A.B. Shinde, S.D. Samant, Study of catalytic activity of free and K10-supported iron oxyhydroxides and oxides in the Friedel-Crafts benzylation reaction using benzyl chloride/alcohol to understand their role in the catalysis by the Fe-exchanged/impregnated K10 catalysts, Appl. Catal. A-Gen. 252 (2003) 23–35.
[16] C. Galindo-Gonzalez, J. de Vicente, M.M. Ramos-Tejada, M.T. Lopez-Lopez, F. Gonzalez-Caballero, J.D.G. Duran, Preparation and sedimentation behavior in magnetic fields of magnetite-covered clay particles, Langmuir 21 (2005) 4410–4419.
[17] L. Dupont, E. Guillon, Removal of hexavalent chromium with a lignocellulosic substrate extracted from wheat bran, Environ. Sci. Technol. 37 (2003) 4235–4241.
[18] U. Förstner, G.T.W. Wittmann, Metal Pollution in the Aquatic Environment, 2nd rev. ed., Springer-Verlag, Berlin/New York, 1981.
[19] J.G. Dean, F.L. Bosqui, K.H. Lanouette, Romoving heavy metals from waste water, Environ. Sci. Technol. 6 (1972) 518–522.
[20] V.K. Gupta, C.K. Jain, I. Ali, M. Sharma, V.K. Saini, Removal of cadmium and nickel from wastewater using bagasse fly ash—a sugar industry waste, Water Res. 37 (2003) 4038–4044.
[21] S. Rengaraj, C.K. Joo, Y. Kim, J. Yi, Kinetics of removal of chromium from water and electronic process wastewater by ion exchange resins: 1200H, 1500H and IRN97H, J. Hazard. Mater. 102 (2003) 257–275.
[22] R. Aravindhan, B. Madhan, J.R. Rao, B.U. Nair, T. Ramasami, Bioaccumulation of chromium from tannery wastewater: an approach for chrome recovery and reuse, Environ. Sci. Technol. 38 (2004) 300–306.
[23] R.R. Patterson, S. Fendorf, M. Fendorf, Reduction of hexavalent chromium by amorphous iron sulfide, Environ. Sci. Technol. 31 (1997) 2039–2044.
[24] M. Pettine, L. D'Ottone, L. Campanella, F.J. Millero, R. Passino, The reduction of chromium (VI) by iron (II) in aqueous solutions, Geochim. Cosmochim. Acta 62 (1998) 1509–1519.
[25] M. Erdem, F. Tumen, Chromium removal from aqueous solution by ferrite process, J. Hazard. Mater. 109 (2004) 71–77.
[26] M.J. Alowitz, M.M. Scherer, Kinetics of nitrate, nitrite, and Cr(VI) reduction by iron metal, Environ. Sci. Technol. 36 (2002) 299–306.
[27] T. Astrup, S.L.S. Stipp, T.H. Christensen, Immobilization of chromate from coal fly ash leachate using an attenuating barrier containing zero-valent iron, Environ. Sci. Technol. 34 (2000) 4163–4168.
[28] J.P. Gould, The kinetics of hexavalent chromium reduction by metallic iron, Water Resour. 16 (1982) 871–877.
[29] T. Lee, H. Lim, Y. Lee, J.W. Park, Use of waste iron metal for removal of Cr(VI) from water, Chemosphere 53 (2003) 479–485.
[30] S.M. Ponder, J.G. Darab, T.E. Mallouk, Remediation of Cr(VI) and Pb(II) aqueous solutions using supported, nanoscale zero-valent iron, Environ. Sci. Technol. 34 (2000) 2564–2569.
[31] R.M. Powell, R.W. Puls, S.K. Hightower, D.A. Clark, Corrosive and geochemical mechanisms influencing in situ chromate reduction by metallic iron, in: 209th ACS National Meeting, American Chemical Society, Anaheim, California, 1995.
[32] A.G.B. Williams, M.M. Scherer, Kinetics of Cr(VI) reduction by carbonate green rust, Environ. Sci. Technol. 35 (2001) 3488–3494.
[33] M. Erdem, F. Gur, F. Tumen, Cr(VI) reduction in aqueous solutions by siderite, J. Hazard. Mater. 113 (2004) 219–224.
[34] A.F. White, M.L. Peterson, Reduction of aqueous transition metal species on the surfaces of Fe(II)-containing oxides, Geochim. Cosmochim. Acta 60 (1996) 3799–3814.
[35] M.L. Peterson, G.E. Brown, G.A. Parks, C.L. Stein, Differential redox and sorption of Cr(III/VI) on natural silicate and oxide minerals: EXAFS and XANES results, Geochim. Cosmochim. Acta 61 (1997) 3399–3412.
[36] H.P. He, R.L. Frost, F. Deng, J.X. Zhu, X.Y. Wen, P. Yuan, Conformation of surfactant molecules in the interlayer of montmorillonite studied by C-13 MAS NMR, Clays Clay Miner. 52 (2004) 350–356.
[37] Y.S. Kang, S. Risbud, J.F. Rabolt, P. Stroeve, Synthesis and characterization of nanometer-size Fe_3O_4 and gamma-Fe_2O_3 particles, Chem. Mater. 8 (1996) 2209–2211.
[38] M.S. Rand, A.E. Greenberg, M.J. Taras, Standard Methods for the Examination of Water and Wastewater, 16th ed., American Public Health Association, New York, 1975.
[39] S.J. Gregg, K.S.W. Sing, Adsorption, Surface Area and Porosity, 2nd ed., Academic Press, London, 1982.
[40] E.P. Barrett, L.G. Joyner, P.P. Halenda, Determination of pore volume and area distribution in porous substances, J. Am. Chem. Soc. 73 (1951) 373–380.
[41] R.M. Cornell, U. Schwertmann, The Iron Oxides: Structure, Properties, Reactions, Occurrences and Uses, Wiley-VCH, Weinheim, 2003.
[42] P. Yuan, H.P. He, F. Bergaya, D.Q. Wu, Q. Zhou, J.X. Zhu, Synthesis and characterization of delaminated iron-pillared clay with meso-microporous structure, Microporous Mesoporous Mater. 88 (2006) 8–15.
[43] J. Mazo-zuluaga, C.A. Barrero, J. Diaz-Teran, A. Jerez, Thermally induced magnetite–haematite transformation, Hyperfine Interact. 148/149 (2003) 153–161.
[44] Q. He, S. Guo, W. Wu, R. Hu, J. Huang, Monodisperse magnetite nanoparticles synthesis and their thermal-stability, in: The 1st International Conference on Bioinformatics and Biomedical Engineering (ICBBE 2007), Wuhan, China, 2007.
[45] P. Yuan, F. Annabi-Bergaya, Q. Tao, M.D. Fan, Z.W. Liu, J.X. Zhu, H.P. He, T.H. Chen, A combined study by XRD, MR, TG and HRTEM on the structure of delam-

inated Fe-intercalated/pillared clay, J. Colloid Interface Sci. 324 (2008) 142–149.
[46] P. Yuan, X.L. Yin, H.P. He, D. Yang, L.J. Wang, J.X. Zhu, Investigation, on the delaminated-pillared structure of TiO_2-PILC synthesized by $TiC1_4$ hydrolysis method, Microporous Mesoporous Mater. 93 (2006) 240–247.
[47] F. Bergaya, B.K.G. Theng, G. Lagaly, Handbook of Clay Science, Elsevier, Amsterdam/London, 2006.
[48] M. Perezcandela, J.M. Martinmartinez, R. Torregrosamacia, Chromium(VI) removal with activated carbons, Water Res. 29 (1995) 2174–2180.
[49] J. Hu, G.H. Chen, I.M.C. Lo, Removal and recovery of Cr(VI) from wastewater by maghemite nanoparticles, Water Res. 39 (2005) 4528–4536.
[50] P.A. Brown, S.A. Gill, S.J. Allen, Metal removal from wastewater using peat, Water Res. 34 (2000) 3907–3916.
[51] S. Babel, E.M. Opiso, Removal of Cr from synthetic wastewater by sorption into volcanic ash soil, Int. J. Environ. Sci. Technol. 4 (2007) 99–107.
[52] S.B. Lalvani, A. Hubner, T.S. Wiltowski, Chromium adsorption by lignin, Energy Source 22 (2000) 45–56.
[53] E. Demirbas, M. Kobya, E. Senturk, T. Ozkan, Adsorption kinetics for the removal of chromium (VI) from aqueous solutions on the activated carbons prepared from agricultural wastes, Water SA 30 (2004) 533–539.
[54] Y.S. Ho, G. McKay, Pseudo-second order model for sorption processes, Process. Biochem. 34 (1999) 451–465.
[55] Y.S. Ho, J.C.Y. Ng, G. Mckay, Removal of lead(II) from effluents by sorption on peat using second-order kinetics, Sep. Sci. Technol. 36 (2001) 241–261.
[56] M.L. Peterson, G.E. Brown, G.A. Parks, Direct XAFS evidence for heterogeneous redox reaction at the aqueous chromium/magnetite interface, Colloid Surf. A 107 (1996) 77–88.
[57] M.L. Peterson, A.F. White, G.E. Brown, G.A. Parks, Surface passivation of magnetite by reaction with aqueous Cr(VI): XAFS and TEM results, Environ. Sci. Technol. 31 (1997) 1573–1576.
[58] J. Manjanna, G. Venkateswaran, Effect of oxidative pretreatment for the dissolution of Cr-substituted hematites/magnetites, Ind. Eng. Chem. Res. 41 (2002) 3053–3063.
[59] F. Magalhaes, M.C. Pereira, S.E.C. Botrel, J.D. Fabris, W.A. Macedo, R. Mendonca, R.M. Lago, L.C.A. Oliveira, Cr-containing magnetites $Fe_{3-x}Cr_xO_4$: The role of Cr^{3+} and Fe^{2+} on the stability and reactivity towards H_2O_2 reactions, Appl. Catal. A-Gen. 332 (2007) 115–123.
[60] E. Tombácz, E. Illés, A. Majzik, A. Hajdú, N. Rideg, M. Szekeres, Ageing in the inorganic nanoworld: example of magnetite nanoparticles in aqueous medium, Croat. Chem. Acta 80 (2007) 503–515.